Biochimica et Biophysica Acta, 1022 (1990) 381–392
Elsevier

BBAMEM 74772

Membrane electroporation – fast molecular exchange by electroosmosis

Dimiter S. Dimitrov * and Arthur E. Sowers

American Red Cross, Holland Laboratory / Cell Biology, Rockville, MD (U.S.A.)

(Received 30 August 1989)

Key words: Electroporation; Electropermeabilization; Electroosmosis; Erythrocyte

Human and rabbit erythrocyte ghosts loaded with FITC-dextran (mol. mass = 10 kDa) and NBD-glucosamine (mol. mass = 342 Da) in buffers of different ionic strength and composition were subjected to electric pulses (intensity 0.7 kV / mm and decay half-time 1 ms) at 7–10 °C and 20–24 °C. The transfer of the fluorescent dyes from the interior of the ghosts through the electropores was observed by low light level video microscopy. The pulses caused the fluorescence to appear outside the membranes as a transient cylindrical cloud directed toward the negative electrode during the first video frame (17 ms). It was similar in both rabbit and human erythrocyte ghosts and at both temperatures but differs for the two dyes, the fluorescence cylinder is long and tall for the FITC-dextran and relatively short and thick for the NBD-glucosamine. The molecular exchange was 2–3 orders of magnitude faster within the first 17 ms after the pulse than the diffusional exchange. It decreased with increasing ionic strength. Formulae for the transfer of molecules by electroosmotic flow through the pores are in agreement with these observations. They allow estimation of the total area of pores with radii larger than that of the fluorescent dye during the pulse. The major conclusion is that electroosmosis is the dominating mechanism of molecular exchange in electroporation of erythrocyte ghosts.

1. Introduction

Application of high-voltage electric field pulses to suspensions of cell membranes induces formation of pores [1–9]. The very existence of pores permits the exchange of molecules across the membrane. It has been commonly assumed that the mechanism of this exchange is diffusional (see, for example, Ref. 10). A diffusional mechanism implies that the rate of molecular transfer through the pores in the membrane depends primarily on the size of pores and molecules, the concentration difference across the membrane and to a lesser extent, the charge on the molecules and the membranes.

Rossignol et al. [11] and Mehrle et al. [12] reported an asymmetrical permeabilization in cells following application of electric pulses. The fluorescent dye was entrapped in the cells predominantly in the hemisphere facing the positive electrode. They attributed this phenomenon to asymmetric formation of pores which leads to asymmetric exchange of the dye by diffusion through the electropores. Later Mehrle et al. [13] showed evidence that the asymmetry was not as high as originally thought. The asymmetrical distribution of pores was attributed to superposition of the intrinsic membrane potential and that induced by the external field [5,12]. However, at field strengths, which induce pore formation, the pulse-induced membrane potential is of the order of 1 V, compared to the intrinsic membrane potential which is of the order of tens of millivolts (Fig. 4 in Ref. 14). Therefore, it is not likely that the very small difference in the net potential (= |induced − intrinsic|) at both hemispheres should lead to such major changes in symmetry of permeabilization.

Recently, Sowers [15] observed that application of electric field pulses to a suspension of erythrocyte ghosts, loaded in the cytoplasmic compartment with FITC-dextran, caused the fluorescence to move from the interior of the ghost and appear as a transient fluorescent cloud just above the membrane hemisphere facing the negative electrode. It had a lifetime of about 200 ms. Sowers also observed that part of the fluorescent cloud could be entrapped in a second, unloaded ghost if that ghost was

* Permanent address: Central Laboratory of Biophysics, Bulgarian Academy of Sciences, Sofia 1113, Bulgaria.

Correspondence: A.E. Sowers, American Red Cross, Holland Laboratory/Cell Biology, 15601 Crabbs Branch Way, Rockville, MD 20855, U.S.A.

in the direction of motion of the label [16]. It was concluded from this second observation that both an influx occurred in all positive electrode facing hemispheres, and an outflux occurred in all negative electrode-facing hemispheres, was induced by an hydrodynamic flow driven by the interaction of the electric field with the positively charged counter-ions at the electropore surfaces (electroosmosis, see, for example, Ref. 17). This flow carried the label towards the negative electrode. This led to the appearance of a cloud of fluorescence only outside the negative electrode-facing hemisphere of the ghost.

The hypothesis for electroosmotic mechanism of asymmetrical redistribution of fluorescence induced by electrical pulses allows an explaination [18] of the data from the experiments where the dye is inside the cell [15] or outside the cell [12] before the pulse is applied. If the tracer molecule is inside the cell then it can exit only through electropores in the hemisphere facing the negative pole. If the tracer molecule is outside the cell then it can enter the cell only through pores facing the positive pole.

Additional evidence that the observation of hemisphere permeability asymmetry is actually an artifact was shown in an experiment where one erythrocyte ghost, loaded with FITC-dextran, was separated by another, which was empty, by a 2–3 μm distance on an axis with the electric field pusle [16]. The loaded ghost released its fluorescent dye through the hemisphere facing the negative electrode, but the empty ghost actually captured a significant amount of fluorescent molecules. This could have happened only if (i) there was a significant amount of electropores in both hemispheres of each ghost, and (ii) electroosmosis caused the efflux in negative electrode facing hemisphere of the loaded ghost and influx in the positive electrode facing hemisphere of the unloaded ghost.

Electroosmosis occurs when an electric field is applied parallel to a charged surface in contact with a solution (see, for example, Refs. 17, 19, 20). The charge on the surface leads to redistribution of the ions in the solution and formation of a double layer, which has thickness of 1 nm to 10 nm for monovalent ion concentrations of 0.1 M to 0.001 M, respectively. The electric field causes motion of the counter-ions in the double layer. This gives rise to hydrodynamic flow. For biological membrane surfaces which are negatively charged the flow is directed towards the negative electrode. The net ion movement causes a hydrodynamic flow of all molecules which are nearby in the solution. McLaughlin and collaborators have shown that electroosmosis is the basis of many important effects in biological systems such as lateral redistribution of membrane proteins [20] and reabsorption of fluid in renal proximal tubules [17].

This paper has four major goals: (1) to present additional experimental evidence and theoretical comparisons for the electroosmotic mechanism of molecular transfer through electropores; (2) to show that the molecular exchange by electroosmosis is much faster than by diffusion; (3) to demonstrate heterogeneity in electropore size and (4) to show possible temperature effects.

The data show that electroosmosis can cause very fast molecular exchange which may be of importance for gene transfer and drug loading [1,21–24].

2. Materials and Methods

Cells and mediums

Human and rabbit erythrocyte ghosts were obtained by hypotonic lysis [25], washed and stored in sodium phosphate buffers (NaP_i) (pH 8.5, 4°C) of different ionic strength (20 mM NaP_i, 60 mM NaP_i or 10 mM NaP_i + 10 mM $MgCl_2$). They were labeled in the cytoplasmic compartment with FITC-dextran (mol. mass = 10 kDa) or NBD-glucosamine (mol. mass = 342 Da) as previously described [15]. Briefly, 1 vol. of 15 mg/ml FITC-dextran in 5 mM NaP_i was mixed with 1 vol. of freshly hemolyzed ghosts in 5 mM NaP_i at 0–4°C. After 1 h this mixture was incubated in 40°C water bath for 2 h. The washing with NaP_i buffer was performed at $10000 \times g$ for 20 min 0–4°C. The ghosts were stored as a pellet in refrigerator. The cell concentration in the suspension used for the experiments was $10 \cdot 10^6$ cells/ml.

Chamber and pulse generator

All observations were made with a rectangular chamber [26]. The pulse generator produced a single exponentially decaying pulse by use of a mercury vapor thyratron as a switch element to discharge a capacitor into the chamber. It is described in detail elsewhere [7]. The pulse strength was 0.7 kV/mm (1.4 kV applied across 2 mm chamber length) and the decay half-time of the pulse was 1 ms. In several experiments the pulse strength was lower, commonly 0.35 kV/mm, or higher (1 kV/mm).

Temperature control

The ambient temperature of the ghost membrane suspension was lowered by introducing liquid nitrogen-cooled air into a styrofoam enclosure surrounding the stage area of the microscope. Viewing and manual access was through windows made of transparent polyethylene sheets with slits or flaps. The temperature was monitored with a dial gauge and thermal stratification was prevented by a small fan inside the enclosure. The stage area was equilibrated to within 5–8°C for at least 20 min before a chamber containing the new cell suspension was loaded onto the stage. Thereafter an additional 5–10 min were allowed for further equilibra-

tion. Some of the experiments were performed at room temperature (22° C).

Fluorescence microscope and TV video system

The observations were made using a Zeiss microscope and recorded on video tape in real time using a Zeiss 3 stage low light level Venus camera for subsequent single frame playback and analysis. The fluorescence at any selected pixel was quantitatively estimated by a Colorado Video (Boulder, Colorado) Model 321 analyzer. The overall system contrast transfer function was determined to be within ± 10% of linearity as a function of specimen location in the viewing field by the use of a series of cytometer fluorescent calibration spheres by Epics (Hialeah, FL). The decrease of fluorescence intensity caused by the electrical pulses was determined by analysis of intensity at the center of each image of fluorescent membrane from single frame playback of sequences recorded on video tape. A Panasonic (Secaucus, NJ) NV-9300A and 499 Video Multimemory (Colorado Video Inc) were used to examine single frames of video sequences. A FORA (West Newton, MA) model VTG-22 video timer operated in the stopwatch mode placed an alpha numeric field with date and time information with 0.01 sec (with ± 0.01 s frame-to-frame accuracy onto each recorded video frame. To determine which recorded frame was immediately before or after a given pulse, a sample of the pulse was used to electronically displace the alpha numeric field to a location about 1 cm above the prepulse location on the monitor screen. Although the video scans were not synchronized with the pulse this system allows resolution in time with respect to exact location of the pulse to be equal to or less than 17 ms. The fluorescence for a given point was measured by placing the intersects of the scan lines of the video analyzer over the center of the ghost image as seen on the monitor. The intensity at all points on the scan line was traced out on the strip chart recorder with intensity as a function of location on the screen. The size of fluorescence clouds was measured by the video analyzer. The frames with image defects as, e.g. lag (see Ref. 27), were discarded. The calibration was performed with a Lafayete objective micrometer and fluorescent calibration spheres.

Protocols

The chambers were filled with a 0.003 ml ghost suspension. One or several pulses were applied. In one type of experiment the polarity of the electrodes was changed after the first or after the second pulse. In another type of experiment the voltage of the second pulse was decreased to half of the first pulse. The fluorescence intensity changes of ghosts were recorded and analyzed by single frame play back of video sequences.

3. Experimental Results

Molecular exchange induced by the pulse

Application of a single pulse to suspension of human ghosts loaded with FITC-dextran (Fig. 1) and NBD-glucosamine (Fig. 2) at 5–8° C led to efflux of fluorescent-tagged molecules from the ghost membranes through all negative electrode-facing hemispheres. This caused a cylindrical-shaped cloud of fluorescence to appear outside the ghost membrane within the duration of one video frame (1/60 s = 16.67 ms) after the pulse. The brightness and volume of this cloud increased to a maximum within approximately the next ten video frames (100–200 ms). Thereafter it faded in brightness while the molecular diffusion caused it to increase in size as fluorescence moved from the cloud to the background. Three qualitative features can be noted in the results (at the two temperatures and when both labels and both human and rabbit ghosts were are used): (1) Regardless of fluorescent marker and regardless of temperature, the cloud brightness increased to a maximum after essentially the same interval (e.g., 100–200 ms) (compare, e.g. Fig. 1 with Fig. 1 in Ref. 15 or with Fig. 3, which is, however, for rabbit ghosts)! (2) The cylindrically shaped cloud of fluorescence from the NBD-glucosamine (Fig. 2) did not grow to the height above the plasma membrane as achieved with FITC-dextran (Fig. 1) but did appear over a larger area (Fig. 2). The FITC-dextran cloud grew as a tall thin cylinder, unlike the NBD-glucosamine one which appeared as a short thick cylinder immediately after the pulse. The later stages of the cloud development were similar for both dyes, slow increase in size in all directions and gradual disappearance. (3) The pulse-induced FITC-dextran cloud for rabbit ghosts at room temperature (Fig. 3) was qualitatively the same as for human ghosts (data not shown but see also Fig. 1 in Ref. 15).

Asymmetry of the fluorescence release

In all experiments the fluorescent cloud appeared outside the membranes above the hemisphere facing the negative electrode (Figs. 1–3). Two different sets of experiments gave additional confirmation of this observation.

In one type of experiment the polarity of the electrodes was changed after the first or after the second pulse. The applied pulses always caused the dye to move towards the negative electrode (see, e.g., Fig. 3 where the polarity of the electrodes was changed after the second pulse). In another type of experiment the second pulse was of lower or higher amplitude than the first pulse. In both cases fluorescent clouds always appeared above the hemisphere which faced the negative electrode.

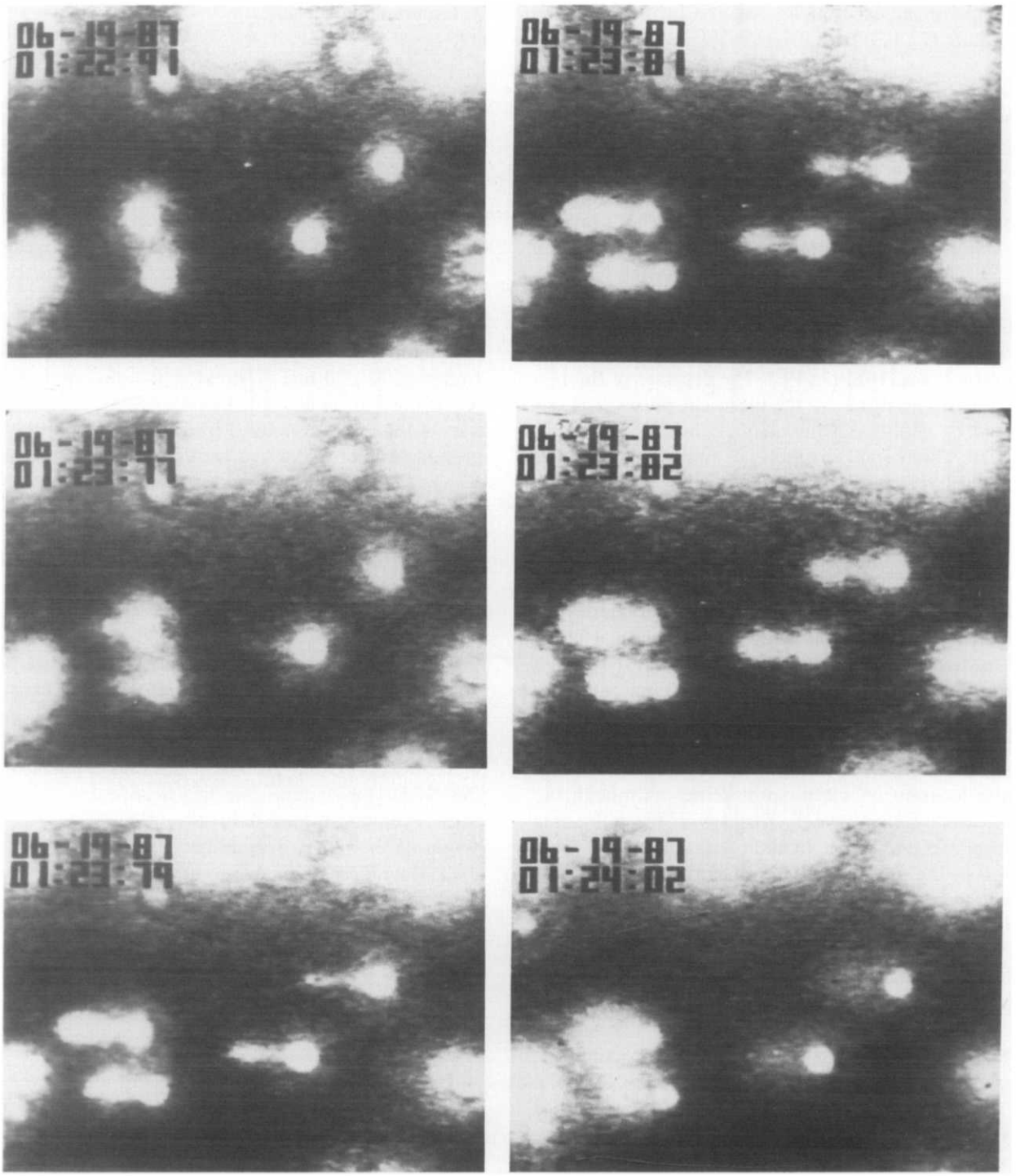

Fig. 1. Appearance of fluorescence clouds after application of a single pulse of 0.7 kV/mm field strength and half-decay time 1 ms on human ghosts, labeled with FITC-dextran (radius 2.3 nm) at low temperature (6 °C). Buffer in medium and cytoplasmic compartments is 20 mM NaP_i (pH 8.5). Alphanumerics: upper, date (month : day : year); lower, time (min : s : hundredths of s). The electric field is parallel to the plane of micrographs. The cloud always appeared toward the negative electrode. Pulse applied at 01 : 23 : 77. The width of the alphanumerics is 50 μm.

Fast molecular exchange during the pulse

Clouds can appear after the application of up to several (typically 1–3) pulses of the same amplitude to the same ghost suspension. Each subsequent pulse resulted in an incremental loss of fluorescence from the interior of the ghost as a transient cloud appeared outside the ghost. The major change in fluorescence intensity of the ghost interior occurred during the pulses and not between them (Fig. 4). It is seen (Fig. 4) that during the first 1–2 frames (20–30 ms) after the first

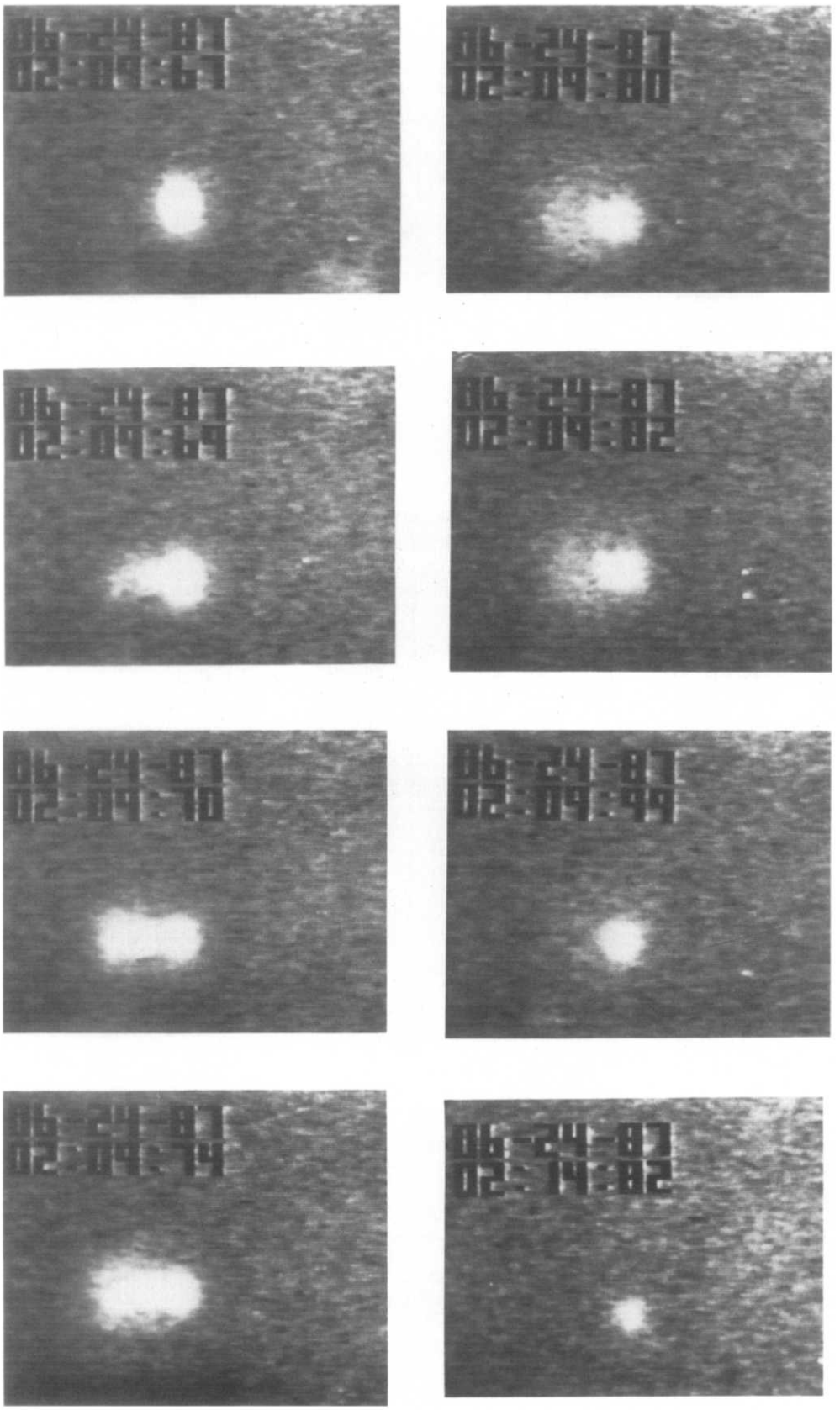

Fig. 2. Effects of a single pulse of intensity 0.7 kV/mm and half-decay time 1 ms applied on human ghosts, labeled with NBD-glucosamine (radius 0.45 nm), at 6 °C. Buffer in medium and cytoplasmic compartments is 20 mM NaP_i (pH 8.5). Alphanumberics: upper, data (month : day : year) lower, time (min : s : hundredths of s). The electric field is parallel to the plane of micrographs. The cloud always appeared toward the negative electrode. Pulse applied at 02 : 09 : 69. The width of the alphanumerics is 50 μm.

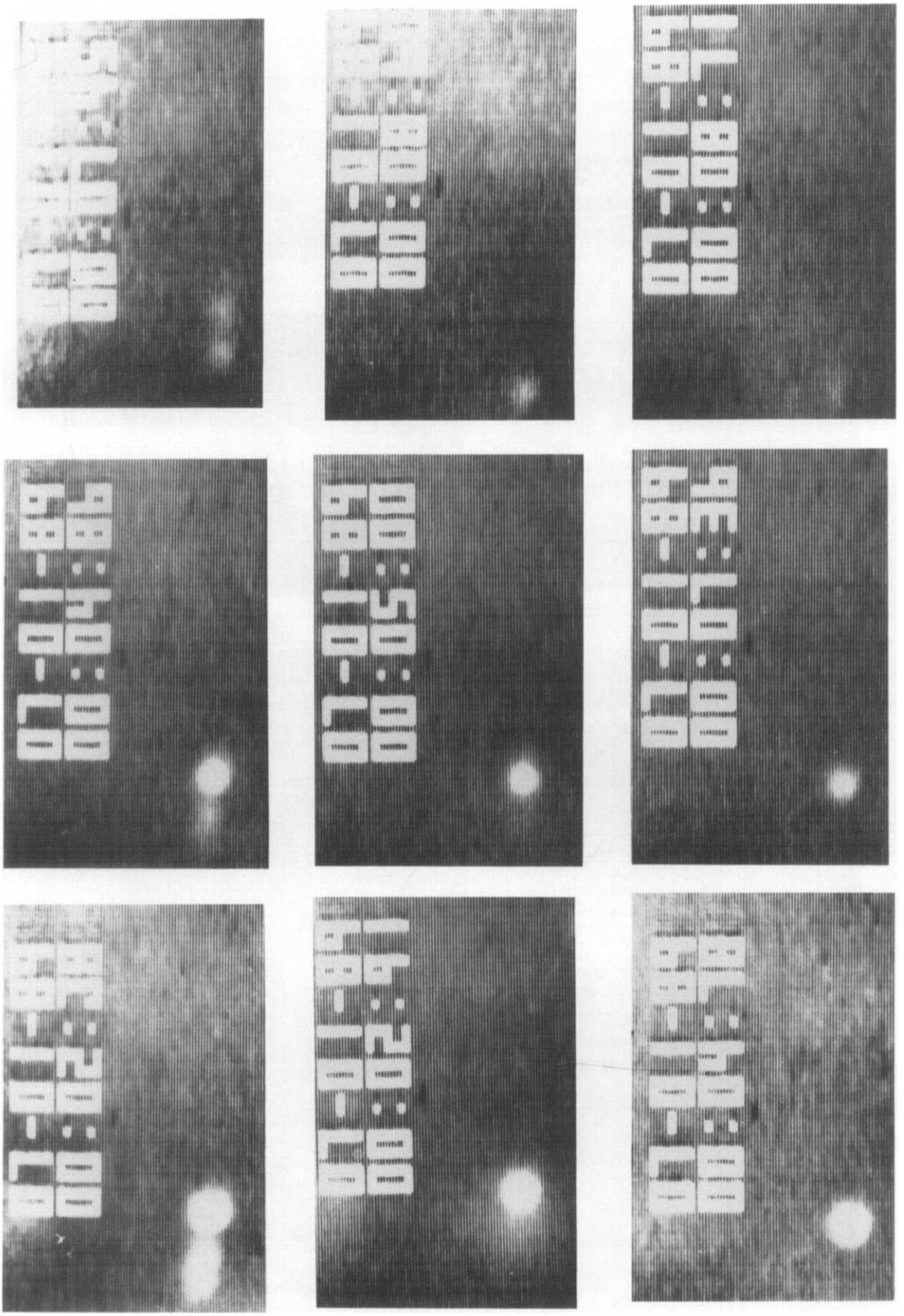

Fig. 3. Fluorescence changes after application of four pulses of intensity 0.7 kV/mm and half-decay time 1 ms on rabbit ghosts, labeled with FITC-dextran (radius 2.3 nm) at room temperature. The polarity of the electrodes was changed for the 3rd and 4th pulse. Buffer in medium and cytoplasmic compartments is 20 mM NaP_i (pH 8.5). Alphanumerics: upper, date (month : day : year); lower, time (min : s : hundredths of s). The electric field is parallel to the plane of micrographs. The cloud always appeared toward the negative electrode. First pulse applied at 00 : 02 : 79. Second pulse at 00 : 04 : 86. Third pulse at 00 : 07 : 45. Fourth pulse at 00 : 08 : 68. The width of the alphanumerics is 50 μm.

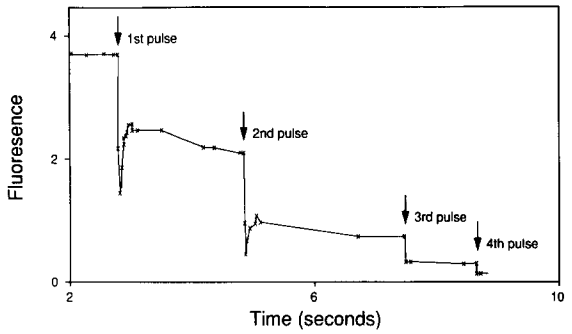

Fig. 4. Dependence of the fluorescent intensity (arbitrary units) for the data shown in Fig. 3 as a function of time. The arrows indicate applications of pulses. The electrode polarity was reversed for the third and fourth pulses. The major change of fluorescence of intensity occurred during and not between the pulses. The experimental error in measuring the fluorescence intensity is less than ± 0.1 . The points represent measurements on selected frames where the intensity change is high. The other measurements are not shown. The resolution in time is one single frame (17 ms).

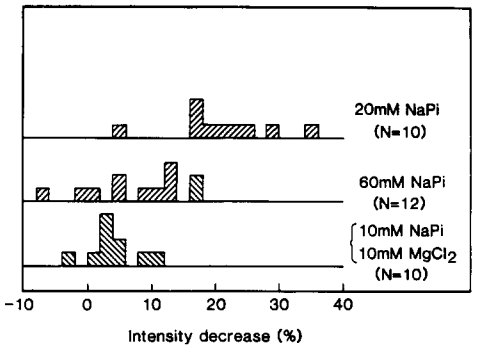

Fig. 5. The increase of ionic strength leads to decrease of the number of ghosts with high fluorescence intensity changes after one pulse. The total number of human ghosts N is 10, 12, and 10 for 20 mM NaP_i, 60 mM NaP_i and 10 mM $NaP_i + 10$ mM $MgCl_2$ buffers, respectively. One square represents one ghost.

pulse the fluorescence intensity inside the ghost decreased to about 40% of the prepulse fluorescence intensity. Then during the next 4–5 frames (70–100 ms) it increased to about 65% of the pre-pulse fluorescence intensity. This increase occurred in most experiments. We interpret this to be due to pulse-induced motion of the whole membrane. This causes an eliptical-shaped blur in the recorded image (commonly several frames after the pulse). The blur represents the same total brichtness spread out over a larger image area. Therefore this results in a decrease in measured intensity at any point in the image. When the membrane motion stops and the image area decreases, the fluorescence at any point increases. The motion of the cells which causes the undershoot in the fluorescence after the pulse can be due to cell electrophoresis, electroosmotic flows in the chamber and/or electrohydrodynamic convection. The fluorescence intensity decreased only by about 15% of the pre-pulse intensity during the next 2 s. This gives approx. 280-times higher rate of fluorescence decrease during the 20–30 ms period after the first pulse than during the next 2 s. The ratio between both rates is even higher for the second and third pulses, respectively 350 and 370. The fourth pulse led to a fluorescence decrease which is comparable with the experimental error (± 0.1). Statistical data for the fluorescent decrease in 32 ghosts at different ionic strengths are presented in the next section. In all ghosts the major change of fluorescence occurred during the pulse.

Molecular exchange decreases at high ionic strengths

Fig. 5 shows the fluorescence intensity decreases induced by a single pulse in single human ghosts for mediums of different ionic strength with monovalent and divalent cations. It is seen that the pulse induced about a 20% decrease in fluorescence in most of the ghosts in 20 mM NaP_i, while for higher ionic concentration (60 mM NaP_i) and for the buffer containing divalent cations (10 mM $NaP_i + 10$ mM $MgCl_2$) the decrease is about 10% and 5%, respectively. The divalent cation led to highest decrease in fluorescence change. The major part of the fluorescence change always occurred during the pulse and not within the period after the pulse when the measurement was done (1 s).

Rate of fluorescent cloud formation

The precise measurement of the rate of formation of the fluorescence cloud during the pulse and immediately after the pulse is limited by: (i) the speed of the video camera (1 frame per 16.67 ms), (ii) the uncertainty due to the fact that the pulse and the video recording system were not synchronized with each other and (iii) image defects as, e.g., lag (see Ref. 27). The micrographs (Fig. 1–3) showed that in all cases the cloud developed its non-diffusional shape (similar to that of a long cylinder) within one frame. The length of

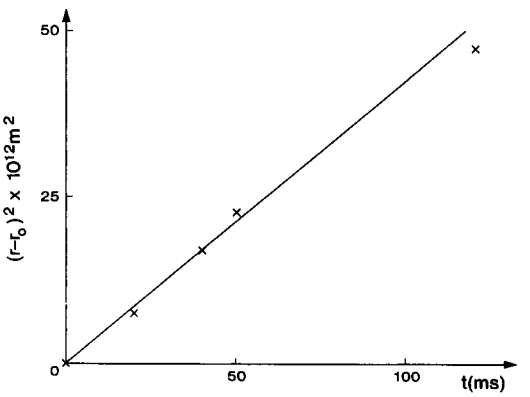

Fig. 6. Dependence of the square of the relative radius of the FITC-dextran cloud on time. The measurements were made from the video frames shown in Fig. 1. The linear dependence at short times indicates diffusional transfer of the fluorescent molecules after the pulse. The derived diffusion coefficient for FITC-dextran is $(1.0 \pm 0.2) \cdot 10^{-6} cm^2/s$.

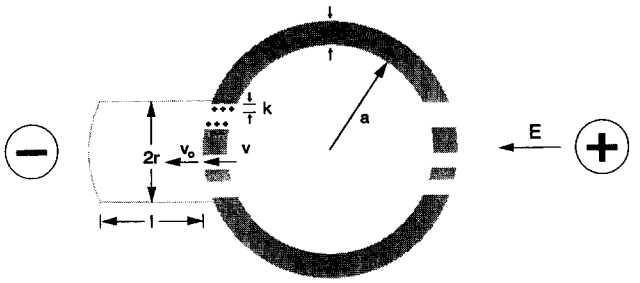

Fig. 7. Sketch of the theoretical model. The ghost is depicted as a spherical membrane of radius a and thickness d. The pulses lead to formation of pores which have total area S and are placed on membrane area A. The ions at the pore walls form a double layer of thickness k. The electroosmotic velocity inside the pore is v and that outside is v_o. The electric field intensity applied by the two electrodes is E_o and that induced across the membrane is E. The electroosmotic velocity v is always towards the negative electrode for negatively charged membrane surfaces.

the fluorescent dye cylinder is typically of the order of the cell radius (about 4 μm). This gives a rate of cylinder growth equal or greater than 0.004 mm/0.017 s = 0.25 mm/s = 250 μm/s.

Fig. 6 shows the diffusion-like increase in radius of the cylindrical cloud with time after the pulse. The cloud was depicted as a cylinder of radius r and length l (see Fig. 7). The initial cloud radius r_0 was measured in the first video frame in which the cloud appeared (Fig. 1, time 01:23:77). The time corresponding to this radius was assumed as a reference time zero. Fig. 7 shows the linear relationship between the square of the difference between the cylinder radius and the initial radius vs. time. It indicates that the mechanism of molecular transfer after the pulse is by diffusion. The diffusion coefficient D for the FITC-dextran derived from the slope of this line (equal to $4D$ for the case of diffusion in one direction (that of the cylindrical coordinate r) (see, for example, Ref. 28)) is $(1.0 + 0.2) \cdot 10^{-6}$ cm^2/s. This value is in reasonable agreement with the value reported in the literature ($0.9 \cdot 10^{-6}$ cm^2/s [29]).

4. Theoretical Model

We consider a cell of radius a (see Fig. 7) exposed to high-voltage pulse of field strength, E_o, and exponential decay half-time, t_p. The pulse leads to formation of n pores of total area S in the membrane of thickness d. The membrane has surface potential, characterized by the zeta potential. The counter-ions form a double layer of thickness k. The external electric field induces electroosmotic flow with average velocity v inside the pore and v_o outside the pore (i.e., the cloud). The electroosmotic flow transfers the fluorescent dye to form a cloud of cylindrical shape (length l and radius r) outside of the ghost. The velocity v inside the pore can be estimated by the Helmholtz-Smoluchowski equation [30,31] (see also Ref. 17).

$$v = \zeta \epsilon E / \mu \tag{1}$$

where the permetivity ϵ, zeta potential ζ and viscosity μ are for the liquid and the membrane surface inside the pore. The field intensity across the pore E is equal to $(1.5aE_o/d)\cos(f)$, f being the angle between the field direction and the direction normal to the membrane surface (see, for example, Ref. 32). At supracritical voltages the actual voltage across the membrane is lower [52]. The above equation for the field intensity across the pore is used only to make estimates. The inertial forces are not taken into account in Eqn. 1. They can be neglected during the pulse when both the Struhal number, $\mathrm{Sh} = mk^2/t_p\mu$ (m is the density of the liquid), which gives the ratio between the non-steady inertial and viscous forces and the Reynolds number, $\mathrm{Re} = mvk/\mu$, which gives the ratio between the steady inertial and viscous forces are smaller than unity (see Ref. 33). For typical values of $m = 1000$ kg/m^3, $k = 3$ nm, $t_p = 1$ ms and $\mu = 0.001$ Pa · s, Sh is of the order of 10^{-8} and Re is of the order of 0.01. Therefore the inertial forces can be neglected in most cases. The velocity v inside the pore can be expressed by the electrophoretic mobility μ if one assumes that the zeta potential inside the pore during electroporation is equal to the zeta potential of the membrane surface. Then Eqn. 1 takes the form (see, for example, 19).

$$v = \mu E \tag{2}$$

This formula can be used only as an estimate when the radii of the pores are comparable or smaller than the double-layer thickness k. In this case it is hard to define the plane of shear and more refined models could give better results. However, the other approximations do not justify the use of more rigorous models.

The volume of liquid, V, which flows out of the porated membrane during the pulse is

$$V = vSt_p \tag{3}$$

This equation is valid both for square and exponentially decaying pulses. In the later case Eqn. 3 was obtained by integration of Eqn. 1 on time, assuming that E is proportional to $\exp(-t/t_p)$. The average velocity outside the pore (in the fluorescent cyclinder) v_o can be calculated from the integral mass balance of medium flowing through the pores during the pulse ($V = vS = v_oA$)

$$v_o = vS/A \tag{4}$$

where A is the cross sectional area of the membrane which has pores. Therefore, S/A gives the part of that porated membrane which is due to pores. The average distance between pores, c, is $(A/n)^{1/2}$, n being the total number of pores. The area A is approximately equal to the cross sectional area of the fluorescent cylinder during the pulse.

The ratio of the molecules transferred by hydrodynamic flows (in our case due to electroosmosis) to those exchanged by diffusion is given by the Peclet's number, Pe, equal to (see, for example, in Ref. 33)

$$\mathrm{Pe} = vd/D \tag{5}$$

The value of the Peclet's number [33] outside the pore is

$$\mathrm{Pe}_o = v_o l/D \tag{6}$$

When Pe > 1 the convective transfer dominates. For our model this means that the molecular exchange is determined by electroosmosis. For Pe < 1, the molecular exchange is due mainly to diffusion.

After the pulse the medium continues to move due to the accumulated kinetic energy. The motion stops after characteristic time

$$t_o = ml^2/\mu \tag{7}$$

During this period of time the average velocity of the medium outside the pore, given by Eqn. 4, drops to zero following an approximately exponential law.

$$v_o = v_{oo} \exp(-t/t_o), \quad v_o = v_{oo} \text{ at } t = 0 \tag{8}$$

These estimates were made by approximating the space derivatives of the velocity in the Navier-Stokes equations with their finite differences (for more details, see Ref. 33).

The hydrodynamic pressure, p, which will be exerted on the membrane around the pore after the pulse is approximately equal to [33]

$$p = mv_o^2/2 \tag{9}$$

This can lead to membrane bending and formation of microfunnels. The experimental conditions are isosmotic. Therefore one can expect that the membrane tension is zero. In this case the membrane resists to bending by its bending elasticity (see, for example, Ref. 34). The extent of membrane bending, b, after the pusle can be estimated by the balance of the hydrodrynamic forces (given by Eqn. 9 and the forces due to bending elasticity (see, for example, Ref. 33)

$$p = mv_o^2/2 = Bb/c^4 \tag{10}$$

where B is the bending elasticity modulus. The membrane bending deformation b, which gives approximately the deviation of the membrane near the pore from the average position of the rest of the membrane can be evaluated by Eqn. 10 as

$$b = mv_o^2 c^4/2B \tag{11}$$

5. Discussion

The sequence of events which leads to release or entrapment of substances in cells by electroporation can be pictured as consisting of four major stages: (1) induction of a high voltage across the membrane; (2) formation and increase in both size and number of pores; (3) transfer of substances through the pores and (4) decreasing in size and number and closing of pores which interrupts the molecular exchange. In this paper we discuss influx and efflux due to electroosmosis during stage 3. It could be expected that electroosmosis can affect the other three stages, but it is beyond the scope of this study.

Electroosmotic molecular exchange

That the molecules exchange by electroosmosis during electroporation is supported by at least six lines of experimental evidence:

(1) The soluble fluorescent dye always moved toward the negative electrode, irrespective of the change of the electrode polarity (Fig. 3). It did so even when the second pulse on the same ghosts was of lower or higher voltage and the electrode polarity was changed. This type of behavior can not be explained by any of the mechanisms which involve interactions of the electric field with induced dipoles, i.e., where the effect depends on the square of the electric field intensity, e.g. dielectrophoresis or changes in the internal pressure due to membrane shape changes. It is also not consistent with formation of pores predominantly on the one hemisphere because in this case the second pulse of higher voltage should produce fluorescence also on the opposite hemisphere. In addition, the second pulse of lower voltage with changed polarity will not be able to produce a transient fluorescent cloud only outside the membrane and facing the negative electrode. Therefore, asymmetric pore formation is unlikely to be the cause of this cloud formation. More likely the cause can be the electroosmotic motion of the positive counter-ions which are in high concentration near the pore walls, which carry negative charges. The concentration of the anions is not high enough to cause motion in the opposite direction.

(2) The shape of the cloud is cylindrical immediately after the pulse (Figs. 1–3). This means that there is vectorial, directed transfer of molecules outside the membrane as is the hydrodynamic flow. Within 100–200 ms after the pulse the shape of the fluorescent cloud resembles that of a sphere, which suggests a diffusional mechanism in the later stages of the cloud development (Fig. 6).

(3) The rate of exchange during the pulse is 2–3 orders of magnitude higher than that after the pulse (Fig. 4). One possibility is formation of many or/and large pores which close very quickly. This can not

explain, however, the asymmetric formation of the fluorescence cloud. Another possibility is electrophoresis of the fluorescent dye. The electrophoretic mechanism can not give such high velocities for substances which are neutral or slightly negatively charged, like the dextran. In addition, it was observed previously [15] that efflux was not observed for some small charged fluorescent dyes.

(4) An increase in the ionic strength caused a decrease in the fluorescent dye efflux (Fig. 5). The increase of the buffer strength from 20 mM to 60 mM led to about one half of the pulse-induced decrease of the fluorescence. The data for the electrophoretic mobility of human red blood cells [35] showed that for these buffer strengths the electrophoretic mobility decreases twice. It should be expected that the electroosmotic velocity can be proportional to the electrophoretic mobility (see Eqn. 2). Therefore the observed decrease of the fluoresence efflux with the increase of the buffer strengthis consistent with the decrease of the electroosmotic molecular exchange.

(5) The heterogeneity in pore size, which was demonstrated with two different fluorescent dyes, does not change the initial rate of growth (i.e., 0.25 mm/s) of the cloud (Figs. 1 and 2). This indicates involvement of hydrodynamic flows and not asymmetric pore formation. In addition, this fact shows that molecular electrophoresis is unlikely to be involved, because the two dyes have different surface properties.

(6) The analysis of the theoretical formulae, based on the electroosmotic mechanism, which follows, agrees semiquantitatively with the experimental observations.

The electroosmotic exchange is very fast

Eqn. 2 predicts that the velocity of the electroosmotic flow through the pore will be high (of the order of 10 m/s), if we assume typical values for the electrophoretic mobility (10^{-8} m^2/Vs) [35]. Measuring the velocity inside the pore is difficult. The estimation of the velocity of the fluorescent cylinder growth, which is higher than 0.25 mm/s, reflects the velocity outside the pore. It can, however, be estimated by the volume of fluorescent cylinder which is formed during the pulse. Eqn. 2, which is based on Eqn. 1 predicts that the cloud volume is proportional to the velocity inside the pore and the total area of pores. Values for the porated area S of the order of 1000 nm^2 [36] and pulse duration 1 ms give cylinder volumes of the order of 1 μm^3, which is in reasonable agreement with experimental findings (Fig. 1). The ratio of the molecules transferred by electroosmotic flow to the diffusional exchange is given by the Peclet's number and is of the order of vd/D (Eqn. 6), which is about 1000. The data shown on Fig. 4 seem to confirm this prediction. It takes less than 17 ms to exchange more molecules by electroosmosis than for periods of seconds by diffusion (Fig. 4).

The velocity outside the pore, estimated by Eqn. 4, is about four orders of magnitude lower. This indicates that the mechanism of molecular transfer during the pulse is electroosmotic in the pore. It is very fast. Outside the pore the transfer occurs by convective and molecular diffusion. It is much slower.

Other possible mechanisms

Other effects could also affect the dye redistribution after the pulse. We estimated the contributions of molecular electrophoresis, pressure changes inside the ghosts due to membrane deformation, inertial forces induced motions and mechanical forces exerted on the membrane which cause its motion. It was not possible to explain our observations with either of these effects. Experiments with fluorescent molecular probes of different charges [15] showed that they always move toward the negative electrode. These observations exclude the molecular electrophoresis as a dominant mechanism. The inertial forces after the pulse can play a limited role because they decay very fast inside the pore, the characteristic decay time is of the order of 1 ps. Our consideration do not exclude the possibility that any of these or other effects contribute to the phenomena of asymmetric dye redistribution during electroporation.

Estimation of pore size distribution

The comparison of the theoretical formulae with the experimental data allows the size distribution of pores during and inmediately after the pulse to be estimated. For example, Eqn. 2 makes it possible to calculate the porated area S. For FITC-dextran ($V = Al = 6$ μm^3) ejected from erythrocyte ghosts one obtains 600 nm^2. This means that there are less than 35 pores which have areas larger than the cross sectional area of dextran (17 nm^2). This is consistent with the recent observations of Chang and Reese [36] who founded less than seven pores (diameters between 25 and 110 nm) per square micron in electrocytes by using a new rapid-freezing technique and a DC off-set radio-frequency pulse (0.5 kV/mm, 100 kHz, 0.1 ms). The volume of the fluorescence cylinder from NBD-glucosamine (radius 0.45 nm) (Fig. 2) is about 5-times larger than those for the FITC-dextran (radius 2.3 nm) (Fig. 1). Therefore the porated area is 3000 nm^2. This gives a number of the order of $(3000-600)/0.63 = 4000$ (0.63 nm^2 is the cross-sectional area of the NBD-glucosamine molecule) pores with radii between 0.45 nm and 2.3 nm. By using fluorescence probes of different radii one can find the size distribution of the pores in the first few ms after the pulse. These estimates, however, should be considered with caution. There is experimental evidence [15] that the charge of the molecules can strongly affect the molecular transfer.

Membrane bending around the pore

Eqns. 10 and 11 predict that after the pulse the accumulated kinetic energy of the hydrodynamic flow will lead to pressure exerted on the membrane around the pore and therefore to membrane bending. Assuming $v_0 = 1$ mm/s, $m = 1000$ kg/m^3, $c = 1$ μm and $B = 10^{-19}$ Nm [34,37] one obtains $b = 10$ nm. This means that microfunnel membrane shapes with heights of the order of 10 nm may be expected, as recently seen by Chang and Reese [36]. The characteristic time for the action of the hydrodynamic force after the pulse is given by Eqn. 7, which predicts values of the order of 1 to 10 ms for cylinder lengths 1 equal to 1 to 3 μm. This shows that the membrane bending is probably short-lived. These estimates are in reasonable agreement with the recent observations [36], which revealed microfunnel structures after electroporation. In addition, because the structures are relatively short-lived (1 to 10 ms according to the above estimate) they can be detected only by fast freezing as in the study of Chang and Reese [36], where the freezing was accomplished within 3 ms. This does not exclude the possibility for microfunnels with longer life-time if there are irreversible changes in the membrane structure and the membrane can not restore its initial shape. There are other possible mechanisms for membrane bending. One of them is exertion of electric forces during the pulse which act normally to the membrane surface (see Eqn. 13 in Ref. 38). In many cases the force which acts on the one side of the membrane can be compensated with that which act on the other side. In these cases there will be no membrane deformation. The problem for membrane deformations during electroporation needs further detailed theoretical consideration and experimental evidence.

Temperature effects

The observations that the dye transfer is not significantly affected by the temperature further indicates that the formation of the fluorescence cylinder is due to pores existing during and immediately after the pulse.

Relations to other studies

To make further development in clarifying electroosmotic and other mechanisms of molecular exchange one needs more knowledge about the mechanisms of pore formation, development and closing. Most of the previous studies which contributed significantly to the understanding of the electroporation mechanism (see, for example, Refs. 3,7–9,38–53 have not taken into account the possibility for electroosmotic effects. On one hand this can lead to underestimation of the molecular exchange during and after electroporation. On the other hand it can affect the current through the pore because of the increased surface conductivity. The electroosmotic flow can also lead to a number of other effects during electroporation. If it is not taken into account the interpretation of the experimental data may not be correct in some cases. If it is taken into account and measured systematically it can provide valuable information about the properties of pores during the pulse. In addition, it may lead to further improvement and optimization of the produce for gene transfer and drug loading.

Conclusions

The major conclusions from this work are: (1) during electroporation the molecules exchange through membranes of human and rabbit erythrocyte ghosts at both low and room temperature by electroosmosis, (2) the electroosmotic effects can provide information about the properties of the electropores during the pulse, (3) the electroosmotic flow leads to much faster molecular exchange than the diffusion, (4) the electropores in erythrocyte ghosts at low temperature are heterogeneous in size and (5) the temperature does not significantly affect the rate of molecular exchange during the pulse. These results can provide a basis for developing new research approaches to investigate electropores and may have applications in gene transfer and drug loading by electroporation [21–24].

Acknowledgements

The expert technical assistance of Ms. Veena Kapoor and Ms. Myoung Soon Cho are gratefully acknowledged. Supported by an American Red Cross fellowship to D.S.D. and the Office of Naval Research contract N00014-89-J-1715 to A.E.S.

References

1 Neumann, E., Schaefer-Ridder, M., Wang, Y. and Hofschneider, P.H. (1982) EMBO J. 1, 841–845.
2 Tsong, T.Y. (1983) Biosci. Rep. 3, 487–505.
3 Dimitrov, D.S. and Jain, R.K. (1984) Biochim. Biophys. Acta 779, 437–468.
4 Knight, D.E. and Scrutton, M.C. (1986) Biochem. J. 234, 497–506.
5 Zimmermann, U., Arnold. W.M. and Mehrle, W. (1988) J. Electrostatics 21, 309–345.
6 Neumann, E., Sowers, A.E. and Jordan, C.A. (1989) Electroporation and electrofusion in cell biology, Plenum Press, New York.
7 Sowers, A.E. (1989) in Electroporation and electrofusion in cell biology (Neumann, E., Sowers, A.E. and Jordan, C.A., eds.), pp. 229–256, Plenum Press, New York.
8 Tsong, T.Y. (1989) in Electroporation and electrofusion in cell biology (Neumann, E., Sowers, A.E. and Jordan, C.A., eds.), pp. 149–163, Plenum Press, New York.
9 Deuticke, B. and Schwister, K. (1989) in Electroporation and electrofusion in cell biology (Neumann, E., Sowers, A.E. and Jordan, C.A., eds.), pp. 127–148, Plenum Press, New York.
10 Michel, M.R., Elgizoli, M., Koblet, H. and Kempf, C. (1988) Experientia 44, 199–203.
11 Rossignol, D.P., Decker, G.L., Lennarz, W.J., Tsong, T.Y. and Teissié, J. (1983) Biochim. Biophys. Acta 763, 346–355.

12 Mehrle, W., Zimmermann, U. and Hampp, R. (1985) FEBS Lett. 185, 89–94.
13 Mehrle, W., Hampp, R. and Zimmermann, U. (1989) Biochim. Biophys. 978, 267–275.
14 McLaughlin, S. (1989) Annu. Rev. Biophys. Biophys. Chem. 18, 113–136.
15 Sowers, A.E. and Lieber, M.L. (1986) FEBS Lett. 205, 179–184.
16 Sowers, A.E. (1988) Biophys. J. 54, 619–626.
17 McLaughlin, S. and Mathias, R.T. (1985) J. Gen. Physiol. 85, 699–728.
18 Sowers, A.E. (1990) in Proc. Int. Symp. Charge and field effects in biosystems (Allen, M., ed.), pp. 315–337, Plenum Press, New York.
19 Balasubraminian, A. and McLaughlin, S. (1982) Biochim. Biophys. Acta 685, 1–5.
20 McLaughlin, S. and Poo, M. (1981) Biophys. J. 34, 85–93.
21 Liang, H., Prurucker, W.J., Stenger, D.A., Kubiniec, R.T. and Hui, S.W. (1988) Biotechniques 6, 550–558.
22 Shikegawa, K. and Dower, W.J. (1988) Biotechniques 6, 742–751.
23 Andreason, G.L. and Evans, G.A. (1988) Biotechniques 6, 650–660.
24 Potter, H. (1988) Anal. Biochem. 174, 361–373.
25 Dodge, J.T., Mitchell, C. and Hanahan, D.J.(1963) Arch. Biochem. Biophys. 100, 119–130.
26 Sowers, A.E. (1984) J. Cell Biol. 99, 1989–1996.
27 Inoue, S. (1986) Video Microscopy, Plenum Press, New York.
28 Dimitrov, D.S., Panaiotov, I., Richmond, P. and Ter-Minassian-Saraga, L. (1978) J. Colloid Interface Sci. 65, 483–494.
29 Granath, K.A. and Kvist, B.E. (1963) J. Chromatogr. 28, 69–81.
30 Helmholtz, H.L. (1879) Ann. Physik. 7, 337–382.
31 Smoluchowski, M. (1921) in Handbuch der Elektrizität und des Magnetismus 2 (Graetz, W., ed.), pp. 366–428, Barth, Leipzig.
32 Lojewska, Z., Farkas, D.L., Ehrenberg, B. and Loew, L.M. (1989) Biophys. J. 56, 121–128.
33 Dimitrov, D.S. (1983) Progr. Surface Sci. 14, 295–424.
34 Berk, D.A., Hochmuth, R.M. and Waugh, R.E. (1989) in Red blood cell membranes: structure, function, clinical implications (Agre, P. and Parker, J.C., eds.), pp. 423–454, Marcel Dekker, New York.
35 Heard, D.H. and Seaman, G.V. (1960) J. Gen. Physiol. 43, 635–654.
36 Chang, D.C. and Reese, T.S. (1989) Biophys. J. 55, 136a–136a.
37 Evans, E.A. (1983) Biophys, J. 43, 27–32.
38 Pastushenko, V.F. (1988) in Biophysics of membrane transport (Kuczera, J. and Przestalski, S., eds.), pp. 13–66, Agricultural University of Wrocław, Wrocław.
39 Neumann, E. (1989) in Electroporation and electrofusion in cell biology (Neumann, E., Sowers, A.E. and Jordan, C.A., eds.), pp. 61–82, Plenum Press, New York.
40 Weaver, J.C. and Powell, K.T. (1989) in Electroporation and electrofusion in cell biology (Neumann, E., Sowers, A.E. and Jordan, C.A., eds.), pp. 111–126, Plenum Press, New York.
41 Sugar, I.P. (1989) in Electroporation and electrofusion in cell biology (Neumann, E., Sowers, A.E. and Jordan, C.A., eds.), pp. 97–110, Plenum Press, New York.
42 Dimitrov, D.S. (1984) J. Membr. Biol. 78, 53–60.
43 Zhelev, D.V., Dimitrov, D.S. and Doinov, P. (1988) Bioelectrochem. Bioenerg. 20, 155–167.
44 Zhelev, D.V., Dimitrov, D.S. and Tsoneva, I. (1988) Bioelectrochem. Bioenerg. 19, 217–225.
45 Chernomordik, L.V., Sukharev, I.G., Popov, V.F., Pastushenko, A.V., Abidor, I.G. and Chizmadzhev, Y.A. (1987) Biochim. Biophys. Acta 902, 360–373.
46 Chernomordik, L.V. and Chizmadzhev, Y.A. (1989) in Electroporation and electrofusion in cell biology (Neumann, E., Sowers, A.E. and Jordan, C.A., eds.), pp. 83–95, Plenum Press, New York.
47 Bliss, J.G., Harrison, G.I., Mourant, J.R., Powell, K.T. and Weaver, J.C. (1988) Bioelectrochem. Bioenerg. 20, 57–71.
48 Needham, D. and Hochmuth, R.M. (1989) Biophys. J. 55, 1001–1009.
49 Sukharev, I.G., Popov, S.V., Chernomordik, L.V. and Abidor, I.G. (1985) Biolog. Membr. 2, 77–86.
50 Weaver, J.C., Harrison, G.I., Bliss, J.G., Mourant, J.R. and Powell, K.T. (1988) FEBS Lett. 229, 30–34.
51 Sugar, I.P., Forster, W. and Neumann, E. (1987) Biophys. Chem. 26, 321–335.
52 Kinosita, Jr., K. Ashikawa, I., Saita, N., Yoshimura, H., Itoh, H., Nagayama, K. and Ikegami, A. (1988) Biophys. J. 53, 1015–1019.
53 Rols, M.-P. and Teissié, J. (1989) Eur. J. Biochem. 179, 109–115.